Electronic Supplementary Material (ESI) for Physical Chemistry Chemical Physics.

Supplementary Information for

Three-body Interaction of Gold Nanoparticles: The Role of Solvent Density and Ligand Shell Orientation

Hari O. S. Yadav

[1] School of Computational and Integrative Sciences, Jawaharlal Nehru University, New Delhi, 110067, India

*Corresponding Author (Email: hariomsyadav@mail.jnu.ac.in, hariyadav.iitd@gmail.com)

Table 1. 12-6 Lennard-Jones parameters of non-bonded interactions for alkanethiol-passivated gold nanoparticles in supercritical ethane.

Atom Types	ε (kJ mol^{-1})	σ (Å)	Refs.
Au	3.2288	2.737	(S1, S2)
SH	1.6629	4.450	(S1, S2)
CH_2	0.3825	3.950	(S3)
CH_3	0.8148	3.750	(S3)

Table 2. Bonded interaction parameters of alkanethiol. Intermolecular bonds are modeled using the harmonic stretching potential; $U(r) = \frac{k_r}{2}(r - r_0)^2$, where k_r is the force constant and r_0 is the equilibrium bond length. Bond angles are modeled using the harmonic bending potential; $U(\theta) = \frac{k_\theta}{2}(\theta - \theta_0)^2$, where k_θ is the force constant and θ_0 is the equilibrium bond angle. The triple cosine potential; $U(\varphi) = \frac{A_1}{2}(1 + \cos(\varphi)) + \frac{A_2}{2}(1 - \cos(2\varphi)) + \frac{A_3}{2}(1 + \cos(3\varphi))$, is employed for 1-4 torsional interactions, where A_1, A_2, and A_3 are constants. The gold-sulfur (Au – SH) interaction is modeled using the switched and shifted version (at 6.2 Å) of pairwise additive $m - n$ potential; $U(r) = \frac{E_0}{(n-m)}\left(m\left(\frac{r_0}{r}\right)^n - n\left(\frac{r_0}{r}\right)^m\right)$; where E_0 is the well depth, r_0 is the equilibrium distance, *m* and *n* are the constants.

Interaction type	Interacting group	Potential parameters[a]	Refs.
Bond	CH_2-CH_x	$k_r = 2250, r_0 = 1.54$	(S3, S4)
	CH_2-SH	$k_r = 2250, r_0 = 1.82$	(S1, S4)
Angle	CH_2-CH_2-CH_x; CH_2-CH_2-SH	$k_\theta = 519.6543$ $\theta_0 = 114$	(S3)
Torsion	CH_2-CH_2-CH_2-CH_x; CH_x-CH_2-CH_2-SH	$A_1 = 5.9038$ $A_2 = -1.1339$ $A_3 = 13.1588$	(S3)
	Au-SH	$E_0 = 38.6$ $r_0 = 2.9$ $m = 4$ $n = 8$	(S2)

[a]The units of distance are in Angstrom, angles in degree and energy in kJ/mol.

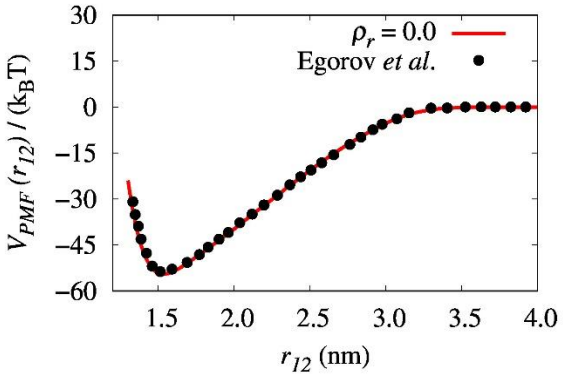

Figure 1. The comparison of two-body PMF of $Au_{38}(SC_{10})_{24}$ nanoparticles computed in vacuum with the literature.[S5]

Table 3. Fitting parameters of pair V_{PMF} curves of two-body and three-body systems at different densities along isotherm, $T_r = 1.02$ for $Au_{38}(SC_{10})_{24}$ and $Au_{140}(SC_{10})_{62}$ nanoparticles. The V_{PMF} curves for densities, $\rho_r \leq 1.0$ are fitted with Morse function, $D_e = \left(\left(1 - \exp\left(-a(r - r_e)\right)\right)^2 - 1\right)$ with $a = \alpha / r_e$, where D_e denotes the energy well depth and r_e represents the equilibrium pair separation. The V_{PMF} curves at density, $\rho_r = 3.0$ are fitted to a function, $B\exp\left(-b(r - r_d)\right)$ with $b = \beta / r_d$, where B is the pre-exponential factor, b characterizes the softness of the PMF curves, and r_d is the onset of repulsion. Both α and β are dimensionless range parameters.

No. of Particles	ρ_r	$Au_{38}(SC_{10})_{24}$			$Au_{140}(SC_{10})_{62}$		
		D_e, B $(k_B T)$	a, b (Å^{-1})	r_e, r_d (Å)	D_e, B $(k_B T)$	a, b (Å^{-1})	r_e, r_d (Å)
Two	0.0	54.64	0.186	15.46	72.61	0.185	25.01
	0.1	45.49	0.164	15.85	58.03	0.165	25.48
	0.5	21.60	0.142	17.15	23.11	0.157	27.82
	1.0	12.98	0.178	17.96	12.15	0.188	28.79
	3.0	2.33	0.398	20.38	2.36	0.367	31.68
Three	0.0	32.86	0.178	17.81	46.98	0.158	26.88
	0.1	28.10	0.164	18.23	38.96	0.155	28.05
	0.5	14.25	0.142	20.14	17.82	0.112	30.97
	1.0	6.48	0.143	21.71	6.71	0.115	33.44
	3.0	1.28	0.328	24.79	1.31	0.319	36.47

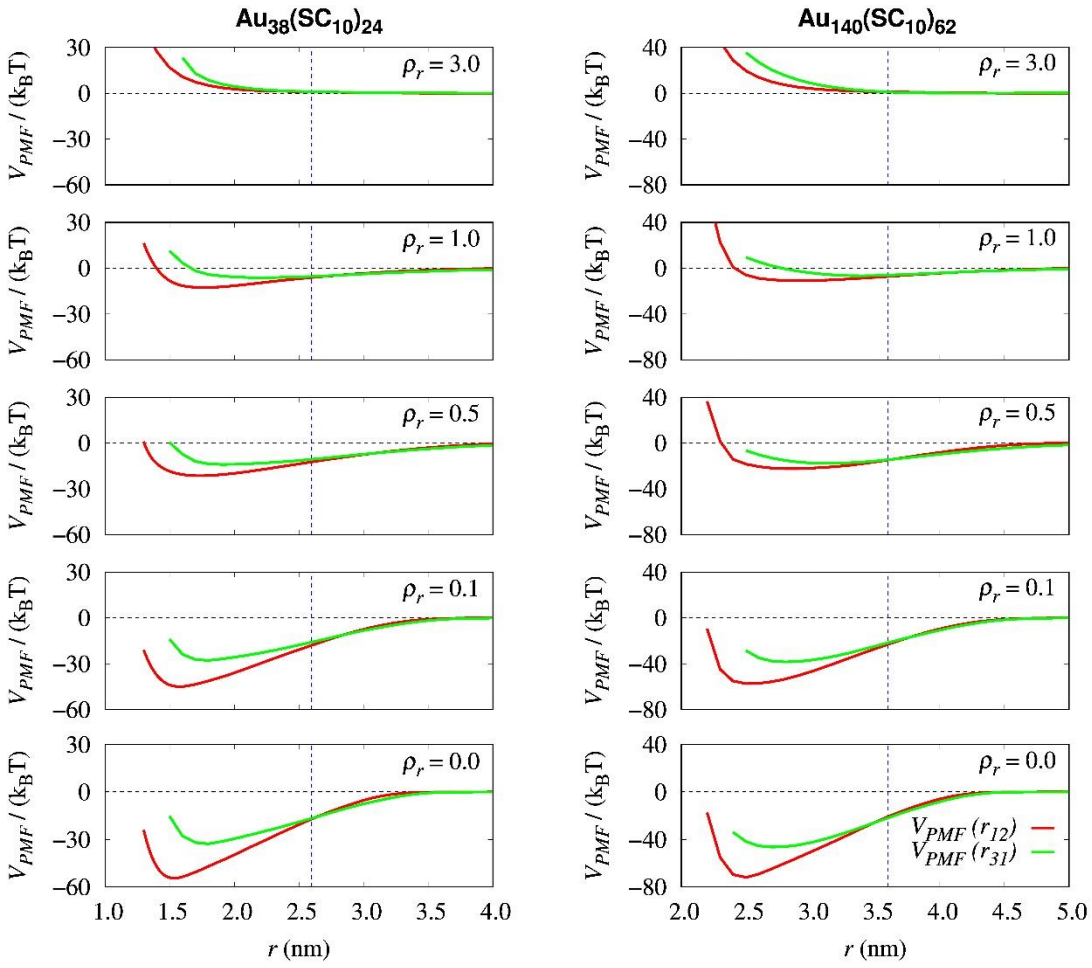

Figure 2. The comparison of $V_{PMF}(r)$ obtained from two- and three-body interactions at different ρ_r for $Au_{38}(SC_{10})_{24}$ (left column) and $Au_{140}(SC_{10})_{62}$ (right column) nanoparticles.

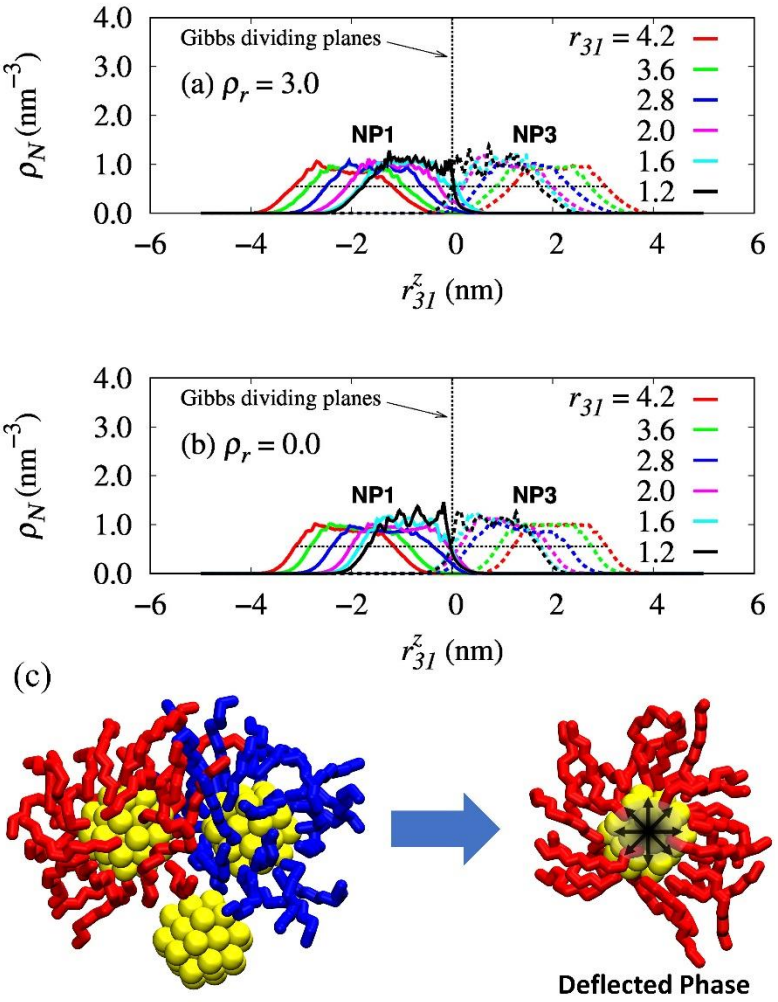

Figure 3. The number density distributions, ρ_N, of ligand shells in three-body interaction along pair separation, r_{31}, at (a) $\rho_r = 3.0$, and (b) $\rho_r = 0.0$, for $Au_{38}(SC_{10})_{24}$ nanoparticles. (c) The visual of deflected phase of ligands at closet separation, i.e., at $r_{31} = 1.2$ nm.

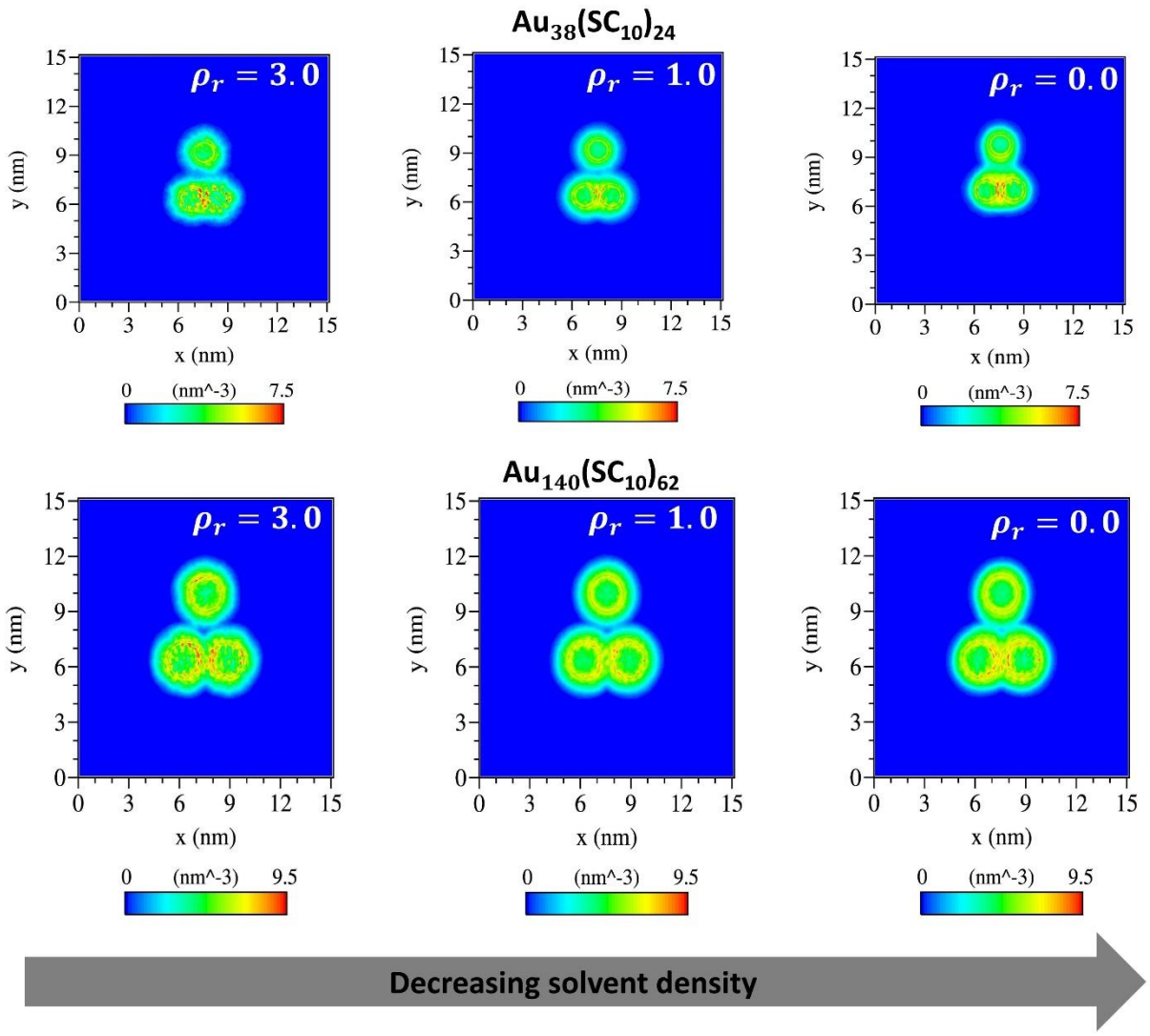

Figure 4. Tow-dimensional density map of ligand shells at intermediate separation as a function of solvent density, ρ_r, for $Au_{38}(SC_{10})_{24}$ (upper row) and $Au_{140}(SC_{10})_{62}$ (lower row) nanoparticles.

REFERENCES

(S1) Landman, U.; Luedtke, W. D. Small Is Different: Energetic, Structural, Thermal, and Mechanical Properties of Passivated Nanocluster Assemblies. *Faraday Discuss* **2004**, *125*, 1–22.

(S2) Tay, K.; Bresme, F. Computer Simulations of Two-Dimensional Gold Nanoparticle Arrays: The Influence of Core Geometry. *Mol Simulat* **2005**, *31* (6–7), 515–526.

(S3) Martin, M. G.; Siepmann, J. I. Transferable Potentials for Phase Equilibria. 1. United-Atom Description of n-Alkanes. *J Phys Chem B* **1998**, *102* (97), 2569–2577.

(S4) Chopra, R.; Truskett, T. M.; Errington, J. R. On the Use of Excess Entropy Scaling To Describe Single-Molecule and Collective Dynamic Properties of Hydrocarbon Isomer Fluids. *J Phys Chem B* **2010**, *114* (49), 16487–16493.

(S5) Patel, N.; Egorov, S. A. Interactions between Sterically Stabilized Nanoparticles in Supercritical Fluids: A Simulation Study. *J Chem Phys* **2007**, *126* (5), 054706.